Interfacial Phenomena and Heat Transfer, 2 (1): 55–74 (2014)

NONLINEAR INSTABILITY OF A THIN FILM FLOWING DOWN A SMOOTHLY DEFORMED THICK WALL OF FINITE THERMAL CONDUCTIVITY

L. A. Dávalos-Orozco

Instituto de Investigaciones en Materiales, Departamento de Polimeros, Universidad Nacional Autonoma de Mexico, Ciudad Universitaria, Circuito Exterior S/N, Delegacion Coyoacan, 04510 Mexico D. F., Mexico; E-mail: ldavalos@unam.mx

The nonlinear instability of a thin film flowing down a heated, sinusoidally deformed thick wall of finite thermal conductivity is investigated. The stabilizing resonant effects of topography obtained in the isothermal case by Dávalos-Orozco (2007, 2008) are investigated along with the stabilizing effects of the thickness and thermal conductivity of the wall found by Dávalos-Orozco (2012). In contrast to the case of a very good thermal conducting wall, the Benney type evolution equation obtained here allows for the presence of topographic effects in the thermocapillary term. In the particular conditions of the problem investigated here, the important result is found that, due to the finite thickness and thermal conductivity of the wall, the film response to the wall deformation decreases in amplitude when the Marangoni number increases. This is due to the extra deformations which appear in the film response in the region near the thinnest part of the wall where its relative thermal conductivity is very high. By contrast, the amplitude of the time-dependent perturbations applied on the free surface increases with the Marangoni number Ma. That is, for fixed initial amplitude, they evolve in time and space to reach a saturation amplitude which increases with Ma. Furthermore, it is shown that it is still possible to stabilize those perturbations in the range of Marangoni numbers investigated when spatial resonance occurs.

KEY WORDS: *thin liquid film, inclined plane, deformed thick wall, Marangoni effect, thermocapillarity*

1. INTRODUCTION

The interest on thin liquid films has increased in recent years due to important applications found in the problems of coating and heat transfer, for example. In the first case it is of interest to have a flat free surface. In the second case, the free surface perturbations might be of interest because the larger the free surface is, the more easily the heat is dissipated [see, for example, Deng et al. (2013)]. The goal of the present paper is to find a way to stabilize a thin fluid layer in the presence of destabilizing thermocapillarity effects due to a temperature gradient across the layer.

Here, in particular, it is of interest to investigate the effects the deformations of a thick wall have on the flow instability. Some papers on this subject have been published in past years in the literature. Experiments have been developed for large-amplitude wall deformation by Zhao and Cerro (1992) and Shetty and Cerro (1993), who found that the position of the liquid free surface has the same period as the wavy wall and a phase shift which depends on the parameters of the flow. The experimental results had good agreement with those obtained from a nonlinear ordinary differential equation for the surface deformation. The theory is checked with experiments by Wierschem et al. (2002).

An analytical linear model has been proposed by Bontozoglou and Papapolymerou (1997) to understand the resonant phenomenon appearing at the free surface due to a particular wavelength of the wall wavy deformations. Wierschem and Aksel (2003) found by a linear stability analysis that the waviness of the wall increases the effective critical Reynolds number in comparison to that of the flow in a flat wall.

Some analytical solutions to the problem with small Reynolds number are proposed by Scholle et al. (2004). They found the creation of vortices when the film thickness and waviness exceed a limit. Numerical boundary-integral

2152–5080/14/$35.00

NOMENCLATURE

A	air jet maximum time-dependent pressure	Re	Reynolds number
a	air jet time-dependent pressure dispersion	S	scaled surface tension number
B	wall deformation amplitude	T	fluid temperature
Bi	Biot number	T_{ambient}	ambient atmosphere temperature
c	phase velocity	T_L	wall lower-face temperature
d	d_{wall}/h_0	T_{wall}	wall temperature
d_{wall}	wall thickness	T_0	zeroth-order fluid temperature
$h(x,y,t)$	film local thickness	u	velocity x-component
$H(x,y,t)$	film local perturbation	U	representative velocity
h_0	unperturbed film thickness	v	velocity y-component
H_h	heat-transfer coefficient	w	velocity z-component
k_c	critical wavenumber		
k_f	fluid heat conductivity	**Greek Symbols**	
k_m	maximum growth wavenumber	β	wall inclination angle
k_s	subcritical wavenumber	Γ	growth rate
k_{wall}	wall heat conductivity	Δ	mean difference
k_x	wavenumber x-component	ε	wave slope smallness parameter
k_y	wavenumber y-component	ζ	wall deformation
L	wall wavelength over perturbation	κ	thermal diffusivity
	wavelength ratio	λ	wavelength
Ma	Marangoni number	ν	kinematic viscosity
p	pressure	ρ	fluid density
P_p	surface external pressure	σ	surface tension
Pr	Prandtl number	Σ	surface tension number
Q_c	wall-over-fluid conductivity ratio	ω	frequency of oscillation

methods are presented by Pozrikidis (1988) for creeping flow. Malamataris and Bontozoglou (1999), by means of numerical analysis, found conditions for flow reversal and a resonance for large Reynolds numbers.

The flow down vertical heated wavy cylinders has been investigated theoretically and experimentally by Negny et al. (2001a,b). Trifonov (1998) uses an integral model to investigate the flow down a wavy wall and found that the numerical solution of this model and that of the Navier-Stokes equations agree for moderate Reynolds number where the instability is due to surface tension.

Valluri et al. (2005) used the integral balance method and found suppression of growth when the wall is corrugated. Kalliadasis et al. (2000) investigated the thin-film response to mounds and cavities with an emphasis on the magnitude of ridges formed at small curvature (steep) regions of the deformed wall. Bielarz and Kalliadasis (2003) present results of films flowing down walls with topography and include the effects of intermolecular forces.

Usha and Uma (2004) made a longwave approximation for the evolution of a viscoelastic thin film down a wavy wall and then used a multiple scale analysis to obtain an evolution equation which has nonlinearity only in one term. Alleborn and Rasziller (2004) investigate a thin film down a wall with topography and under the action of an external localized pressure. Dávalos-Orozco (2007) found, in a numerical analysis in space and time of a Benney-type equation including smooth wall deformations, that it is possible to stabilize the time-dependent perturbations imposed on the free surface by means of sinusoidal wall deformations. This phenomenon is a spatial resonance due to the large-amplitude response of the free surface to the waviness of the wall. This resonance produces a local decrease of the

thickness of the layer that takes the time-dependent perturbations into a region where the flow is stable. The important point is that the stabilizing effect is so strong that the perturbations cannot recover in the next crest of the free surface response and the perturbation fades away in space and time. Dávalos-Orozco (2008) has shown that this effect can also occur for finite spatial extension of the waviness of the wall and that even a small deformation like a one-dimensional pit or hole may have an important influence on stability in a long spatial range. This problem has been extended to a viscoelastic upper-convected fluid layer by Dávalos-Orozco (2013b). Note that by means of an integral method, Trifonov (2007a) also found stabilizing results due to sinusoidal deformation of the wall. Trifonov (2007b) confirmed this by means of the the numerical solution of the Navier-Stokes equations and found instability when the wave and wall wavelength are similar.

Other papers have appeared in the literature discussing the stabilizing effect of the wavy wall. Oron and Heining (2008) used the weighted-residual integral boundary layer model for this problem. Wierschem et al. (2008) found new results regarding the spatial resonance due to a wavy wall by means of linear theory. Heining et al. (2009a), by solving numerically the full steady nonlinear Navier-Stokes equations, found bistable resonance and the coupling of lower harmonics and wall deformation to generate higher harmonics. D'Alessio et al. (2009) present an approximation to the problem which is combined with the weighted-residual integral boundary layer model and find that for weak and moderate surface tension the wavy wall stabilizes, but for strong surface tension it destabilizes. Heining and Aksel (2009b), based on the free surface deformations, propose a method to determine the bottom profile. Hacker and Uecker (2009) propose a weighted-residual integral boundary layer equation for the solution of the problem. They are able to describe vortices in the troughs of the wavy wall with a better precision than before. Pascal and D'Alessio (2010) present a combination of the effects on stability of the waviness of the wall and its permeability. Heining and Aksel (2010) apply the effects of a sinusoidal wall to the stability of a non-Newtonian power-law fluid. The formation and presence of eddies due to the wall deformation was investigated by Scholle et al. (2008). The possible stabilization of the vortices was studied by Wierschem et al. (2010). They found that the increase of Reynolds number produces a decrease in the size of the vortices, which may disappear if its magnitude is large enough. Gambaryan-Roisman et al. (2011) used the integral boundary layer method to investigate the stability of the film under three-dimensional meandering wall deformations. Heining et al. (2012) investigated the effects of corrugations of the wall on pattern formation and on laminar mixing. The stability of the film was investigated by Veremieiev et al. (2012) under the action of an external electric field. Cao et al. (2013) present experiments with the goal to understand even more the behavior of thin films falling down a deformed wall. They found a new instability mode due to short traveling waves. Pollak and Aksel (2013) present experimental results of the linear stability of a film going down a wavy wall. They use steep undulations to calculate the stability branches. Heining et al. (2013) investigated the inverse problem of calculating the wall topography and free surface deformation by measuring one component of the free surface velocity.

Some papers have been published in relation to the Marangoni instability. Alexeev et al. (2005) present experiments and numerical analysis on Marangoni phenomena with a horizontal deformed wall. They found the possibility of rupture of the film, as well as in the paper by Kabova et al. (2006). Saprykin et al. (2007) made a lubrication approximation and found an accumulation of liquid in the troughs due to the higher surface tension.

Recently, D'Alessio et al. (2010) calculated the stability of a thin film falling down a heated wavy wall. It was assumed that the wall is a very good heat conductor. Use was made of the weighted-residual method to calculate a nonlinear equation to describe the evolution of the free surface perturbations. They also present in their appendix a Benney-type equation, including topography and thermal Marangoni effects, under the assumption of a very good thermal conducting wall; however, they do not present solutions of that nonlinear equation. The numerical solutions have been calculated and presented in Dávalos-Orozco (2013a). Ogden et al. (2011) extended this problem to include porosity in the wavy wall.

The thickness and thermal conductivity of the wall have been used by a few authors. Oron et al. (1996) needed to use the thickness of the wall to eliminate singularities at the rupture point in a problem of thermal and evaporative instabilities. Kabova et al. (2006) included in their thermal Marangoni problem wall topography and finite thickness and conductivity of the wall. Gambaryan-Roisman et al. (2010) investigated a thermocapillary problem of a liquid layer over a thick wall with variable thermal conductivity. The variation of the thickness of the wall is only done assuming a relation with the thermal conductivity nonuniformity. Gambaryan-Roisman and Stephan (2009) investigated

the formation of rivulets in thin films flowing down a heated thick wall with topography and taking into account the Lennard-Jones potential, but only longitudinal undulations are used.

Dávalos-Orozco (2012) investigated extensively the problem of Kabova et al. (2006) and Gambaryan-Roisman (2010) in the case of a thin film flowing down a flat wall with finite thickness and thermal conductivity. It is shown that the ratio d/Q_C of the wall-liquid thicknesses ratio d over the wall-liquid conductivities ratio Q_C plays a very important stabilizing roll with regard to the flow.

Here, the goal is to investigate the combined effects of wall topography, finite thickness, and thermal conductivity of the wall. It is of interest because, as shown first by Kabova et al. (2006) in the lubrication approximation, when the wall is thick the deformations introduce a new factor in the thermocapillary term of the evolution equation. This factor disappears when the wall is a very good conductor. Therefore the thermocapillary term reduces to the same one found in the evolution equation for a flat, thick, very well conducting wall calculated by Dávalos-Orozco (2012) and found in Eq. (A3) of D'Alessio et al. (2010).

In the present paper it is of great concern to find the parameter range where the spatial resonance occurs and the possibility of stabilizing the flow, including the thickness of the wall. Rupture phenomena is not taken into account (see, for example, Ajaev, 2013). The evolution equation will be calculated under the lubrication approximation (Benney, 1966; Joo, et al., 1991a,b; Joo and Davis, 1992; Dávalos-Orozco et al., 1997; Dávalos-Orozco and Busse, 2002; Dávalos-Orozco, 2007, 2008), including a thermocapillary term. Therefore the stabilizing effect of the isothermal sinusoidal wall at spatial resonance might be more difficult to attain (Dávalos-Orozco, 2007, 2008). The limitations of the lubrication approximation model have been investigated in Schied et al. (2005).

The paper is structured as follows. In the next section, the perturbed Benney equation is calculated, including thermocapillarity, wall deformation, finite thickness, and thermal conductivity. In Sec. 3, numerical solutions of the equation are presented. Sections 4 and 5 are the Discussion and Conclusions, respectively.

2. PERTURBED BENNEY EQUATION WITH THERMOCAPILLARITY, WALL DEFORMATION, FINITE THICKNESS, AND THERMAL CONDUCTIVITY

In this section the perturbed Benney equation is calculated, including the effects of the thick wall deformation and thermocapillarity. The coordinate system used is related with that of the flow down a flat wall, where the main velocity component is in the x-direction, which is perpendicular to the z-direction crossing the film thickness and pointing outwards from the fluid film (see Fig. 1). The lower face of the wall is located at $z = -d_{\rm wall}$, where $d_{\rm wall}$ is the thickness of the wall. The y-direction is perpendicular to these two, assuming the system is right handed. This is used as a reference coordinate system to set the wall deformations and the free surface deformations appearing as a response to the wall profile.

The approximation is based on $\varepsilon = 2\pi h_0/\lambda \ll 1$, which is the small parameter. Here, the thickness of the layer is represented by h_0 and the effective wavelength by λ, which is supposed to be very long. Therefore the slope of the free surface deformations is small. It is assumed that the wall deformations satisfy the same conditions. The nondimensionalization is done by means of h_0 for distance in the z-direction, $\lambda/2\pi$ for distance in the x- and y-directions, $h_0\lambda/(\nu 2\pi)$ for time, ν/h_0 for velocity, $\rho\nu^2/h_0^2$ for pressure, and $\triangle T = (T_L - T_{\rm ambient}) > 0$ for temperature. Here, ν is the kinematic viscosity and ρ is the density. Besides, T_L is the temperature at the lower face of the wall, and $T_{\rm ambient}$ is the temperature of the ambient atmosphere above the fluid free surface.

If the unperturbed free surface is set at $z = \zeta(x, y) + 1$, then the perturbed free surface is located at $z = \zeta(x, y) + 1 + H(x, y, t) = \zeta(x, y) + h(x, y, t)$. The function $H(x, y, t)$ is the film local perturbation. Here, $\zeta(x, y)$ is the wall deformation. The wall lower face is found at $z = -d = -d_{\rm wall}/h_0$.

If the angle of inclination of the wall is β, ${\rm Re} = gh_0^3/\nu^2$ is the Reynolds number and the Prandtl number is ${\rm Pr} = \nu/\kappa$ (where κ is the fluid thermal diffusivity). The nondimensional and scaled Navier-Stokes, continuity, and heat diffusion equations are

$$\varepsilon u_t + \varepsilon u u_x + \varepsilon v u_y + w u_z = -\varepsilon p_x + \varepsilon^2 u_{xx} + \varepsilon^2 u_{yy} + u_{zz} + {\rm Re}\sin\beta, \tag{1}$$

$$\varepsilon v_t + \varepsilon u v_x + \varepsilon v v_y + w v_z = -\varepsilon p_y + \varepsilon^2 v_{xx} + \varepsilon^2 v_{yy} + v_{zz}, \tag{2}$$

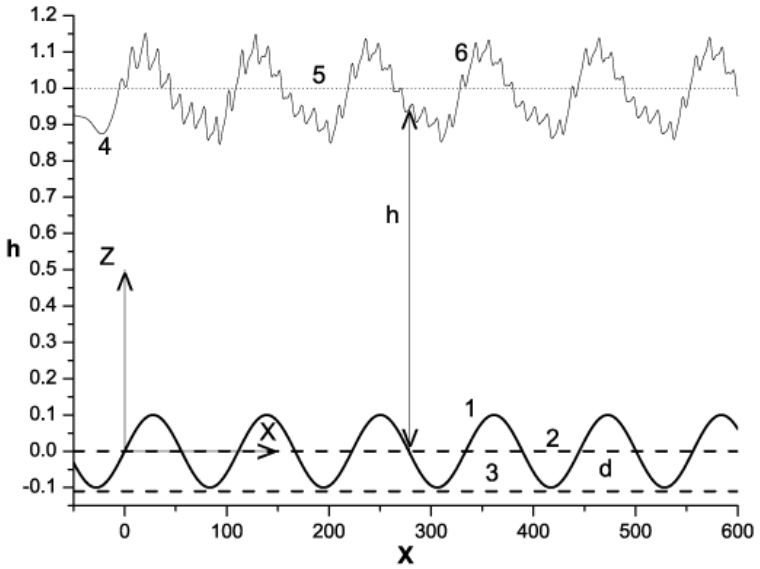

FIG. 1: Vertical wall and thin film system. The mean non dimensional wall thickness is $d = 0.11$, (1) Wall sinusoidal deformation (solid), (2) Mean height of the wall (dashed), (3) Lower side of the wall located at $z = –0.11$ (dashed) with non dimensional temperature 1, larger than that of the atmosphere above the free surface, (4) Free surface response to the wall deformation, (5) Mean height of the unperturbed free surface (dotted), (6) Time dependent perturbations excited at $x = 0$ and running on the free surfaces response. They have a local height $h(x, t)$ with respect to the wall deformation. The largest and smallest thickness of the wall are 0.21 and 0.01, respectively.

$$\varepsilon w_t + \varepsilon u w_x + \varepsilon v w_y + w w_z = -p_z + \varepsilon^2 w_{xx} + \varepsilon^2 w_{yy} + w_{zz} - \mathrm{Re}\cos\beta, \tag{3}$$

$$w_z = -\varepsilon u_x - \varepsilon v_y, \tag{4}$$

$$\mathrm{Pr}\,(\varepsilon T_t + \varepsilon u T_x + \varepsilon v T_y + w T_z) = \varepsilon^2 T_{xx} + \varepsilon^2 T_{yy} + T_{zz}. \tag{5}$$

$$\frac{\nu}{k_{\mathrm{wall}}}\varepsilon T_{\mathrm{wall}t} = \varepsilon^2 T_{\mathrm{wall}xx} + \varepsilon^2 T_{\mathrm{wall}yy} + T_{\mathrm{wall}zz}. \tag{6}$$

Subindexes x, y, z, and t indicate partial derivatives. The variables in the equations are as follows: (u, v, w) are the velocity components in the (x, y, z) directions, p is the pressure, T is the temperature, T_{wall} is the wall temperature, and k_{wall} is the wall thermal diffusivity. The boundary conditions are evaluated at the wall and at the free surface. At the wall, the nonslip condition is

$$u = v = w = 0 \qquad \text{at } z = \zeta(x, y), \tag{7}$$

where $\zeta(x, y)$ is the smooth wall deformation [see Dávalos-Orozco (2007)]. Note that when $\zeta(x, y) = 0$ the wall is flat. The normal stress boundary condition is

$$\begin{aligned} &-p + \frac{1}{N^2}\left[\varepsilon^3(u_x f_x^2 + v_y f_y^2) + \varepsilon^3(u_y + v_x) f_x f_y - \varepsilon(v_z + \varepsilon w_y) f_y - \varepsilon(u_z + \varepsilon w_x) f_x + w_z\right] = P_p(x, y, t) \\ &-\frac{3}{N^3} S[(1 + \varepsilon^2 f_y^2) f_{xx} + (1 + \varepsilon^2 f_x^2) f_{yy} - 2\varepsilon^2 f_x f_y f_{xy}] \quad \text{at} \quad z = \zeta(x, y) + h(x, y, t), \end{aligned} \tag{8}$$

where $f(x, y, t) = \zeta(x, y) + h(x, y, t)$ and $N = \sqrt{1 + \varepsilon^2 f_x^2 + \varepsilon^2 f_y^2}$. Here $f(x, y, t)$ is the total height of the free surface with respect to the origin of the coordinate system. $h(x, y, t)$ is the location of the free surface relative to the local wall deformation and its magnitude varies around the nondimensional thickness 1. In the absence of time periodic perturbations [see Eq. 14)], $h(x, y, t)$ is a response of the fluid layer due to surface tension and shear stresses

appearing when $\zeta(x,y) \neq 0$. The tangential shear stresses are not zero due to the shear stresses produced by the changes of surface tension caused by the imposed temperature gradient. They are

$$\varepsilon(w_z - \varepsilon u_x)f_x - \frac{1}{2}\varepsilon^2(u_y + v_x)f_y + \frac{1}{2}(u_z + \varepsilon w_x)(1 - \varepsilon^2 f_x^2) - \frac{1}{2}\varepsilon^2(\varepsilon w_y + v_z)f_x f_y = \frac{\mathrm{Ma}}{\mathrm{Pr}}(\varepsilon T_x + \varepsilon h_x T_z)$$
$$\text{at} \quad z = \zeta(x,y) + h(x,y,t), \tag{9}$$

and

$$\varepsilon(w_z - \varepsilon u_y)f_y - \frac{1}{2}\varepsilon^2(u_y + v_x)f_x + \frac{1}{2}(v_z + \varepsilon w_y)(1 - \varepsilon^2 f_y^2) - \frac{1}{2}\varepsilon^2(\varepsilon w_x + u_z)f_x f_y = \frac{\mathrm{Ma}}{\mathrm{Pr}}(\varepsilon T_y + \varepsilon h_y T_z)$$
$$\text{at} \quad z = \zeta(x,y) + h(x,y,t). \tag{10}$$

The temperature conditions are

$$T_{\mathrm{wall}} = 1, \quad \text{at} \quad z = -d$$
$$T_{\mathrm{wall}} = T \quad \text{and} \quad Q_c dT_{wall}/dz = dT/dz, \quad \text{at} \quad z = 0 \tag{11}$$

$$T_z + \mathrm{Bi}(T+1) = 0 \quad \text{at} \quad z = \zeta(x,y) + h(x,y,t), \tag{12}$$

where $\mathrm{S} = \varepsilon^2\Sigma$ and $\Sigma = \sigma h_0/(3\rho\nu^2)$ is the nondimensional surface tension number with σ the surface tension. The ratio of the wall and fluid heat conductivities is represented by $Q_c = k_{\mathrm{wall}}/k_f$. The Biot number is $\mathrm{Bi} = H_h h_0/k_f$, where H_h is the coefficient of heat transfer. The Marangoni number is defined as $\mathrm{Ma} = (-d\sigma/dT)\triangle T h_0/(\rho\nu\kappa)$. The scaling used in the definition of S implicitly assumes that surface tension is very strong. The kinematic boundary condition is

$$w = \varepsilon h_t + \varepsilon u f_x + \varepsilon v f_y \quad \text{at} \quad z = \zeta(x,y) + h(x,y,t). \tag{13}$$

Notice that a pressure $P_p(x,y,t)$ appears in the normal stress boundary condition Eq. (8). This pressure is supposed to be applied on the free surface from the ambient air in the form of a turbulent jet. The goal is to use it to control locally the position and frequency of the time-dependent perturbations applied on the thin film. That pressure will be assumed to have the form

$$P_p(x,y,t) = A\left|\sin\frac{\omega}{2}t\right|\exp[-a(x^2+y^2)]. \tag{14}$$

In the numerical calculations, this turbulent air jet will be striking periodically on the free surface around the origin. For applications of a nonoscillating turbulent air slot jet (plane jet) see Lacanette et al., (2006). In a turbulent air jet the impingement pressure profile on the free surface has the form of a Gaussian (Lacanette et al., 2006). The meaning of the constants A and a of the pressure P_p in Eq. (14) is the following. A represents the maximum air jet pressure on the surface, and the inverse of the square root of a represents the spreading range of the jet on the surface. As will be seen below in the evolution Eq. (19), this pressure $P_p(x,y,t)$ is operated by a second derivative in space. Therefore the constants A and a will appear multiplied as Aa^2. In the numerical analysis of Eq. (19), this product may produce large-amplitude deformations on the free surface. This effect avoids the fast saturation of the time-dependent perturbation in a short space interval, mainly when the saturation amplitude is small. For this reason, and after some trial numerical calculations, the decision was to fix the magnitudes of those constants as $A = 0.0001$ and $a = 0.05$. Here, ω is the frequency of oscillation, which is divided by two because a jet has no suction (therefore the absolute value of the sine function), and it will be effective only when it strikes again (with positive sign) on the surface.

Now, the variables are expanded as

$$u = u_0 + \varepsilon u_1 + \cdots, \qquad v = v_0 + \varepsilon v_1 + \cdots, \qquad w = \varepsilon(w_1 + \varepsilon w_2 + \cdots),$$
$$p = p_0 + \varepsilon p_1 + \cdots, \qquad T = T_0 + \varepsilon T_1 + \cdots, \qquad T_{\mathrm{wall}} = T_{\mathrm{wall0}} + \varepsilon T_{\mathrm{wall1}} + \cdots. \tag{15}$$

The above expansions are used in the equations of motion, continuity, heat diffusion, and boundary conditions. Here, due to their importance, only the results for the main temperature profiles are presented. They are

$$T_{w0} = \frac{Q_C\left[1 + \mathrm{Bi}h(x,y,t)\right] - \mathrm{Bi}\left[z - \zeta(x,y)\right]}{Q_C\left[1 + \mathrm{Bi}h(x,y,t)\right] + \mathrm{Bi}\left[d + \zeta(x,y)\right]} \tag{16}$$

$$T_0 = \frac{Q_C\left[1+\mathrm{Bi}h(x,y,t)\right]-\mathrm{Bi}Q_C\left[z-\zeta(x,y)\right]}{Q_C\left[1+\mathrm{Bi}h(x,y,t)\right]+\mathrm{Bi}\left[d+\zeta(x,y)\right]} \tag{17}$$

Notice that T_{w0} equals one at $-d$ and equals T_0 at $z=\zeta(x,y)$. The heat flux boundary condition is also satisfied at $z=\zeta(x,y)$. At the lowest order the free surface deformation satisfies

$$h_t = -\,\mathrm{Re}\sin\beta h^2\frac{\partial h}{\partial x} \quad \text{at} \quad z=\zeta(x,y)+h(x,y,t). \tag{18}$$

At the next order, the result is an evolution equation of the Benney type for the free surface deformation of a thin film flowing down an inclined thick wall with smooth deformations. That is

$$h_t+\mathrm{Re}\sin\beta h^2h_x+\varepsilon\left\{(\mathrm{Re}\sin\beta)^2\left(\frac{2}{15}h^6h_x\right)_x+\frac{1}{3}\nabla\cdot\left[h^3\left[-\mathrm{Re}\cos\beta\nabla(\zeta+h)+3\mathrm{S}\nabla^2\nabla(\zeta+h)-\nabla P_p\right]\right.\right.$$
$$\left.\left.+\frac{3}{2}\frac{\mathrm{Ma}}{\mathrm{Pr}}\frac{\mathrm{Bi}h^2\left[\nabla h+\dfrac{1}{Q_C}\nabla\zeta\right]}{\left(1+\mathrm{Bi}\left[h+\dfrac{1}{Q_C}\zeta+\dfrac{d}{Q_C}\right]\right)^2}\right]\right\}=0. \tag{19}$$

Here, $\nabla=(\partial/\partial x,\partial/\partial y)$ is the horizontal nabla operator. It is clear that when $\zeta(x,y)=0$, this equation reduces to that obtained by Dávalos-Orozco (2012). However, when $Q_C\to\infty$ (very good conducting wall), this equation reduces to Eq. (A3) in the appendix of D'Alessio et al. (2010). Notice that there the wall deformation is missing in the thermocapillary term. In the same limit but when the wall is flat, $\zeta=0$ and $\mathrm{Ma}=0$, the equation reduces to a perturbed Benney equation (Dávalos-Orozco et al., 1997). Moreover, if also $P_p=0$ the equation reduces to that of Benney (1966) (see also Joo et al., 1991; Joo and Davis, 1992). In the case $P_p=0$ and $\mathrm{Ma}>0$, the equation reduces to that used by Joo et al. (1991) when their evaporation number $E=0$ (no evaporation). They use a parameter K which is 1/Bi, the inverse of the Biot number.

The smoothness required by the wall deformations becomes clear from Eq. (19), where $\zeta(x,y)$ must have continuous derivatives until the fourth order. This restriction is satisfied by a sinusoidal function. Equation (19) will be solved numerically in the next section for the particular sinusoidal wall profile and a fixed wall thickness.

The linear problem is solved as in Dávalos-Orozco (2012), that is, assuming small perturbations of the form $H(x,t)=A_1\exp i[kx-(i\Gamma+\omega)t]$, where A_1 is a small constant amplitude. Here, k is the wavenumber, Γ is the growth rate, and ω is the frequency of oscillation. In this way, the result is that the linear phase velocity is $c=\omega/k=\mathrm{Re}\sin\beta$, which depends on the Reynolds number and that the linear growth rate is

$$\Gamma=k^2\left(\frac{2\,\mathrm{Re}^2\sin^2\beta}{15}-\frac{1}{3}\,\mathrm{Re}\cos\beta-k^2\Sigma+\frac{1}{2}\frac{\mathrm{Ma}}{\mathrm{Pr}}\frac{\mathrm{Bi}}{\left[1+\mathrm{Bi}+\mathrm{Bi}\left(\dfrac{d}{Q_c}\right)\right]^2}\right). \tag{20}$$

When the growth rate is zero, the curve of criticality is

$$k_c=\sqrt{\frac{1}{\Sigma}\left(\frac{2}{15}\,\mathrm{Re}^2\sin^2\beta-\frac{1}{3}\,\mathrm{Re}\cos\beta+\frac{1}{2}\frac{\mathrm{Ma}}{\mathrm{Pr}}\frac{\mathrm{Bi}}{\left[1+\mathrm{Bi}+\mathrm{Bi}\left(\dfrac{d}{Q_c}\right)\right]^2}\right)}. \tag{21}$$

It is easy to show that the wavenumber of the linear maximum growth rate is $k_m=k_c/\sqrt{2}$, the same relation as in the isothermal case. Gjevik (1970) calculated the nonlinear curve of subcriticality below which the solutions of Eq. (19) could not saturate. Gjevik [see also Dávalos-Orozco and Busse, 2002; Dávalos-Orozco, 2012)] has shown the nonlinear result $k_s=k_c/2$. The nonlinear calculations including the Marangoni effect and wall properties have been done by Dávalos-Orozco (2012), who found the same relation $k_s=k_c/2$ [see Eq. (21)] as in the isothermal case.

It has been shown numerically (Joo et al., 1991; Dávalos-Orozco et al., 1997) in the isothermal case that saturation can be found below but near the curve of subcriticality. The presence of thermocapillary effects makes it more difficult to attain saturation below subcriticality for large enough Marangoni numbers. The above results are reviewed as follows:

$$k_c = \sqrt{2}k_m = 2k_s. \tag{22}$$

The importance of the factor $f(d/Q_C, \mathrm{Bi}) = \mathrm{Bi}/[1 + \mathrm{Bi}(1 + d/Q_C)]^2$ has been examined in Dávalos-Orozco (2012). That function is plotted in Fig. 2(a). Curves for Bi $= 0.1$ and Bi $= 1$ are shown in Fig. 2(b). As can be seen in Fig. 2(b), when Bi $= 1$ the magnitude of this term is larger for small d/Q_C, in particular, when $d/Q_C = 0$. Above the magnitude $d/Q_C = 2.162$, the curve is lower than that of Bi $= 0.1$. This means that when Bi $= 1$, the linear perturbations are easier to stabilize for $d/Q_C > 2.162$. All this is valid in the problem of the flat wall. When the wall presents sinusoidal deformations, new terms appear in the thermocapillary factor of Eq. (19), one in the numerator $\nabla\zeta(x, y)/Q_C$ and another one in the denominator $\zeta(x, y)/Q_C$. Note in Eq. (19) that the thermocapillary factor still needs to be operated by the ∇ found in front of the large brackets. Therefore the new Eq. (19) in fact has two extra terms in comparison with that found by Dávalos-Orozco (2012) and with Eq. (A3) in the appendix of D'Alessio et al. (2010). One corresponds to the spatial derivative of the numerator and another one to the spatial derivative of the denominator. It is important to observe that in those extra terms the derivatives of $\zeta(x, y)/Q_C$ appear in the numerators and that they may have an important influence on the nonlinear stability. In particular, $\zeta(x, y)/Q_C$ becomes important when Q_C is small, and its derivatives are more important for small but relatively large magnitudes of the wave number of the wavy wall. The discussion of the numerical results is given below, where calculations are done for particularly relevant magnitudes of the parameters.

3. NUMERICAL ANALYSIS OF EQ. (19)

The numerical analysis of Eq. (19) is done in space and time using finite differences of first order in time and centered finite differences of second order in space. Only variations in the x-direction are assumed in the calculations. The initial conditions for the numerical calculations are that $H(x, t) = \partial H(x, t)/\partial x = 0$ at the beginning and at the end of the spatial interval. At each time step the full spatial range is calculated. The results at a given time are recovered

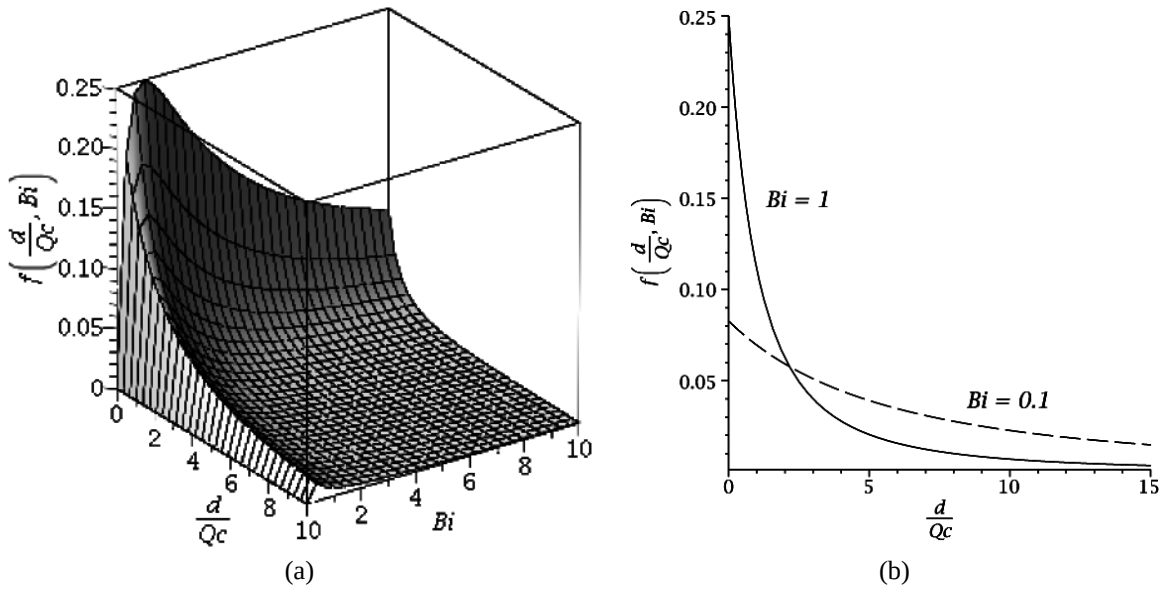

FIG. 2: (**a**) Graph of the function f(d/Q_C, Bi) = Bi/(1 + Bi + Bid/Q_C)^2; (**b**) Plot of f(d/Q_C, Bi) for the particular values of Bi $= 0.1$ (dashed) and Bi $= 1$ (continuous).

as initial conditions for the next time step. In this way, the time-dependent perturbations are found to travel in space and time.

The following parameters are fixed to the values Pr = 7, S = 1, and β = 90° (for a vertical wall) in all the calculations. The wall deformation will always be sinusoidal, and its wavelength will be changed in relation to the wavelength of the time-dependent perturbation imposed on the free surface. The wall sinusoidal wavelength is determined as in $\zeta(x) = B\sin[xk/L]$, where $k = \omega/\mathrm{Re}\sin\beta$ is the wavenumber corresponding to a given ω, Re and β. As will be shown below, ω and Re will be selected, just for reference, as those corresponding to the maximum growth rate of the isothermal problem. It is clear that the wavelength of the wall deformation is taken as L times (with L a real number) the wavelength $\lambda = 2\pi/k = 2\pi\mathrm{Re}\sin\beta/\omega$ produced by the time-dependent surface perturbation. B is the wall deformation amplitude which will be fixed as 0.1. The goal of taking the wall wavenumber as L times λ is to have an easy way to find the spatial resonance where perturbations are damped and stabilized, as found by Dávalos-Orozco (2007) in the isothermal case. It is assumed that the wall deformation is zero at $x = 0$, where the time-dependent perturbation is applied. The numerical calculations are in space and time, and will start in a spatial location $x =$ –100 until a location $\mathrm{Re}\sin\beta\Delta t$ + 100 determined by the $\mathrm{Re}\sin\beta$, which is the phase velocity, and by the time interval Δt required. Therefore, it is necessary to determine from the onset the evolution time interval needed to investigate a particular perturbation in order to know the spatial distance required for the numerical calculations. The added 100 spatial units are necessary to avoid artificial reflection of the perturbations at the end of the interval.

Spatial resonance occurs when a particular magnitude of L produces a free surface response with a very large amplitude, which locally reduces the film thickness in such a way that the local Reynolds number is so small that the time-dependent perturbations enter a region where they are stable and unable to grow again in space and time (Dávalos-Orozco, 2007). As in the previous paper, the resonance stabilizing effects can be found for any Reynolds number if the Marangoni number is not too large, and the Biot number is not very important in the new complex thermocapillary term of Eq. (19).

In the numerical results, only Reynolds numbers corresponding to the maximum growth rate of the isothermal case will be used as a reference for the given frequency ω of the time-dependent perturbation. The calculations show that when the ratio d/Q_C is large, the Marangoni effects are stabilized as in Dávalos-Orozco (2012), even when the factor $1/Q_C$ of the wall deformation is large. Therefore, after checking different regions of the parameters ω and Re, it was decided to fix Bi = 0.1 and $d = 0.11$ in order to understand the behavior of the factor $\zeta(x, y)/Q_C$ and its derivatives in the thermocapillary term. Besides, two examples will be provided for Bi = 1. The two magnitudes $Q_C = 0.01$ and $Q_C = 0.05$ are used. This means that the wall thermal conductivity is 100 and 20 times smaller than that of the fluid, respectively. As explained above, the amplitude of the waviness of the wall is fixed as $B = 0.1$ and consequently the thickness of the wall oscillates between 0.01 and 0.21. This contrast is relevant in the phenomena shown in the following figures. The assumed magnitude of B is a consequence of the introduction of the wall-fluid interface deformation into the lubrication approximation. Table 1 helps to separate the fixed from the varying parameters used in the numerical calculations. Notice that in each pair of figures presented below, the first one corresponds to L out from resonance and the second one to (stabilizing) resonance.

3.1 Results for Bi = 0.1

The results are given starting from small frequencies ω of the time-dependent perturbations imposed on the free surface. They correspond to a perturbation frequency ω = 0.5, ω = 1, and ω = 2.

3.1.1 Case for ω = 0.5 and Re = 1.391

In this way, Fig. 3 shows results when ω = 0.5 and Re = 1.391, for $Q_C = 0.01$ and 0.05. In this case the wavenumbers are above the curve of subcriticality for the Marangoni numbers used. Notice that for the sake of presentation, a

TABLE 1: Fixed and Variable Parameters

Fixed	$A = 0.0001$	$a = 0.05$	$B = 0.1$	$d = 0.11$	Pr = 7	S = 1	β = 90°	ε = 0.1
Variable	Bi	L	Ma	Q_C	Re	ω		

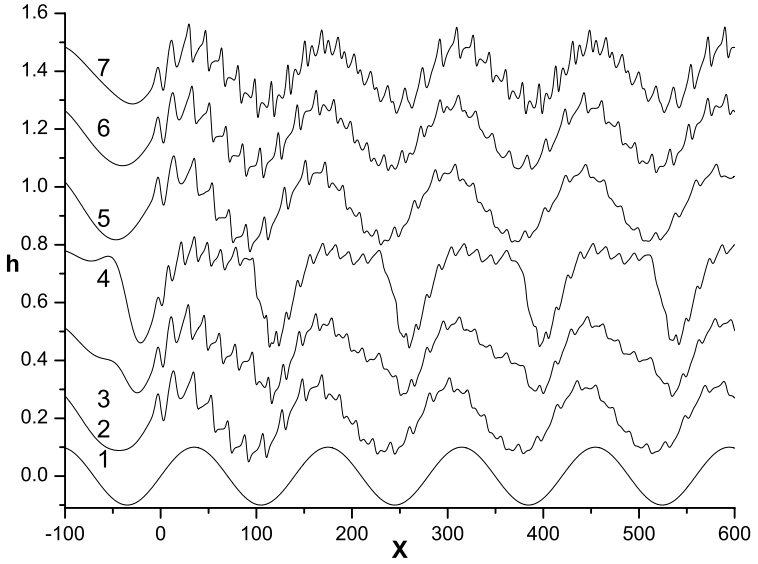

FIG. 3: Pr $= 7$, S $= 1$, Bi $= 0.1$, $d = 0.11$. $\omega = 0.5$, Re $= 1.391$, $L = 8$. (1) Wall. $Q_C = 0.01$: (2) Ma $= 10$, (3) Ma $= 50$, (4) Ma $= 100$. $Q_C = 0.05$: (5) Ma $= 10$, (6) Ma $= 50$, (7) Ma $= 100$. Notice pure responses from $x =$ –100 to 0.

number of free surface numerical results are plotted in only one figure. The mean distance of the wavy wall to the deformed free surface is 1 in all the figures of the paper, as shown in Fig. 1. The wavy wall profile is shown as an important reference with respect to its own influence on the free surface deformations, isothermal and nonisothermal. Both magnitudes of Q_C are very small and the wall is relatively a bad heat conductor with respect to the liquid layer. As discussed in Dávalos-Orozco (2012) for a flat wall, the flow stabilizes when d/Q_C increases, as shown in Fig. 2. However, here the stability and response of the free surface to the wall waviness depends not only on Q_C, but also on the ratio $[\zeta(x) + d]/Q_C$, which in some places is small, as can be seen in curve 1 of Fig. 3 representing the wavy wall. In other places the wall is thicker than the mean. To each magnitude of Q_C corresponds three curves for Ma $= 10$, 50, and 100. The time-dependent perturbations are applied at $x = 0$ on the free surface. Notice that the pure response of the free surface to the wavy wall can be seen to the left of $x = 0$, the origin of the x-axis. One hundred space units, from –100 to 0, are given to observe with detail the response without the superposition of perturbations. It is interesting that for each magnitude of Q_C the amplitude of the response decreases when Ma increases, in contrast with the numerical results presented in Dávalos-Orozco (2013a) for a very good conducting wall. This is due to the deformation (the bump) which appears in the free surface response near the thinnest part of the wall and near the valley of the response. That thinnest part is where the wall presents the highest effective thermal conductivity, which as seen, has a relevant influence on the film response. Therefore the finite thickness and the low conductivity of the wall are responsible for these phenomena. It is important to note in Fig. 4 that even under these circumstances, it is still possible to stabilize the time-dependent perturbations by means of spatial resonance for $L = 5$ (lower than that of Fig. 3).

3.1.2 Case for $\omega = 1$ and Re $= 1.967$

Figures 5 and 6 correspond to $\omega = 1$ and Re $= 1.967$. The wavenumbers are above the curve of subcriticality for the three magnitudes of Ma. As can be seen, the free surface response also decreases with Ma. The bump due to the thinnest part of the wall appears again in Fig. 5 with $L = 9$. In contrast, in Fig. 6 for $L = 6$, it appears to the right of the valley of the response. It is clear from Fig. 6 that the time-dependent perturbations are considerably reduced due to spatial resonance.

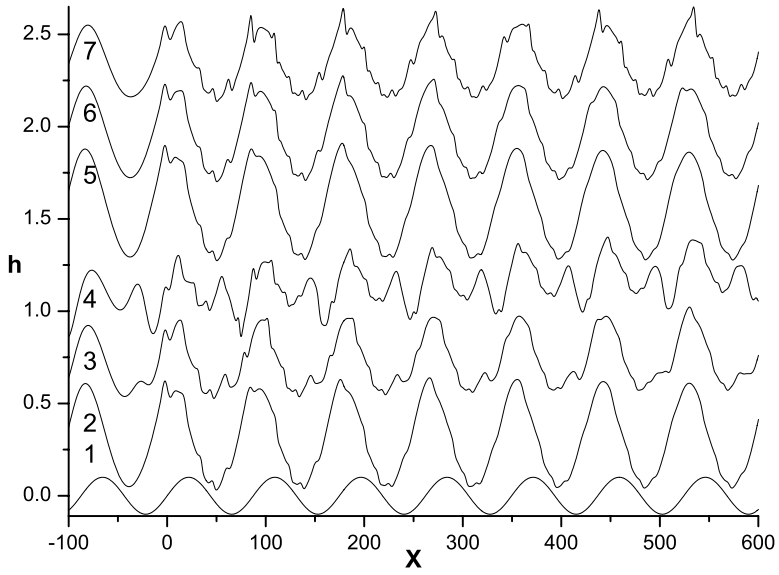

FIG. 4: The same as Fig. 3, but $L = 5$. The free surface response decreases with Ma. Resonance. Notice pure responses from $x =$ –100 to 0.

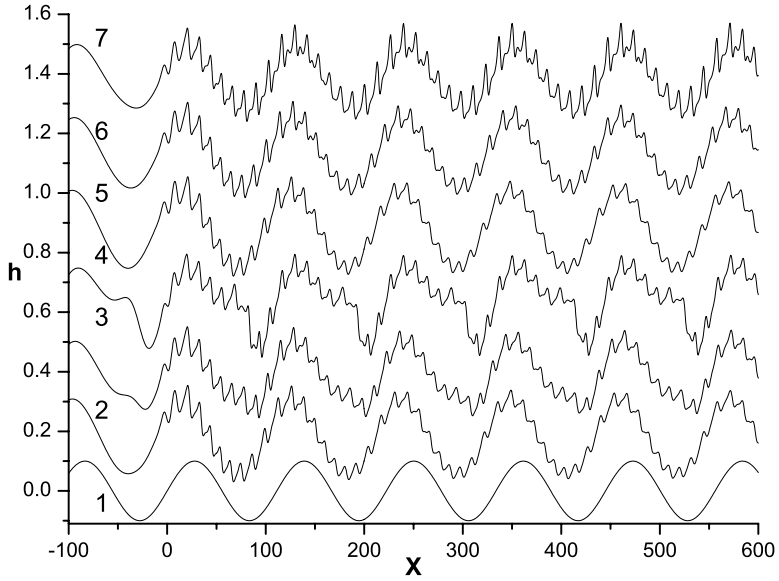

FIG. 5: Pr $= 7$, S $= 1$, Bi $= 0.1$, $d = 0.11$. $\omega = 1$, Re $= 1.967$, $L = 9$. (1) Wall. $Q_C = 0.01$: (2) Ma $= 10$, (3) Ma $= 50$, (4) Ma $= 100$. $Q_C = 0.05$: (5) Ma $= 10$, (6) Ma $= 50$, (7) Ma $= 100$. Notice pure responses from $x =$ –100 to 0.

3.1.3 Case for $\omega = 2$ and Re $= 2.783$

An increase to $\omega = 2$ and Re $= 2.783$ leads to the results of Figs. 7 and 8. Here, too, the wavenumbers are above the curve of subcriticality. As before, the amplitude of the free surface response decreases with Ma. It is evident that the

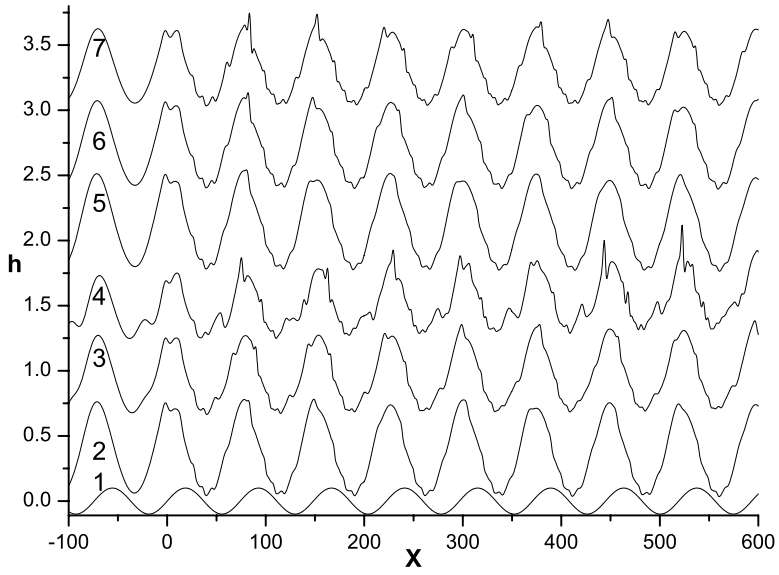

FIG. 6: The same as Fig. 5, but $L = 6$. The free surface response decreases with Ma. Resonance. Notice pure responses from $x =$ –100 to 0.

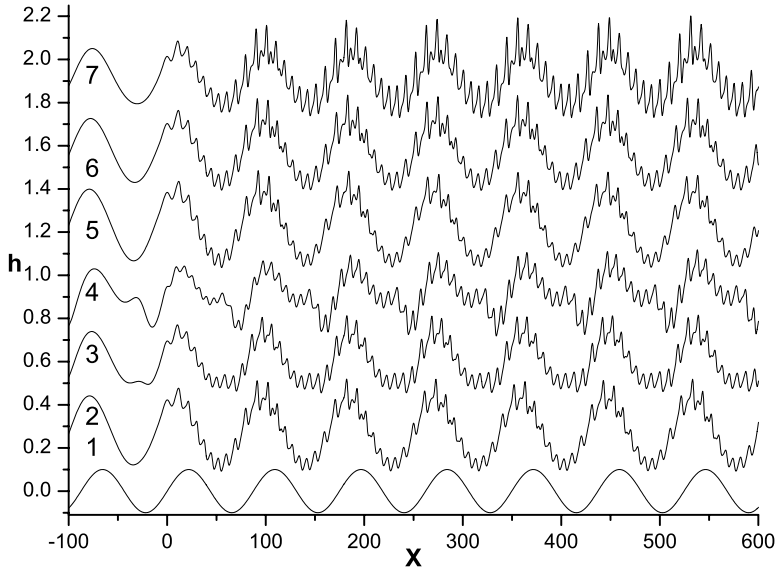

FIG. 7: Pr $= 7$, S $= 1$, Bi $= 0.1$, $d = 0.11$. $\omega = 2$, Re $= 2.783$, $L = 10$. (1) Wall. $Q_C = 0.01$: (2) Ma $= 10$, (3) Ma $= 50$, (4) Ma $= 100$. $Q_C = 0.05$: (5) Ma $= 10$, (6) Ma $= 50$, (7) Ma $= 100$. Notice pure responses from $x =$ –100 to 0.

effect of the thinnest part of the wall is to create a bump which widens the valley of the free surface response when Ma increases. Observe in Fig. 8 that the perturbations for Ma $= 100$ are easier to stabilize when $Q_C = 0.05$ (curve 7) than when $Q_C = 0.01$ (curve 4).

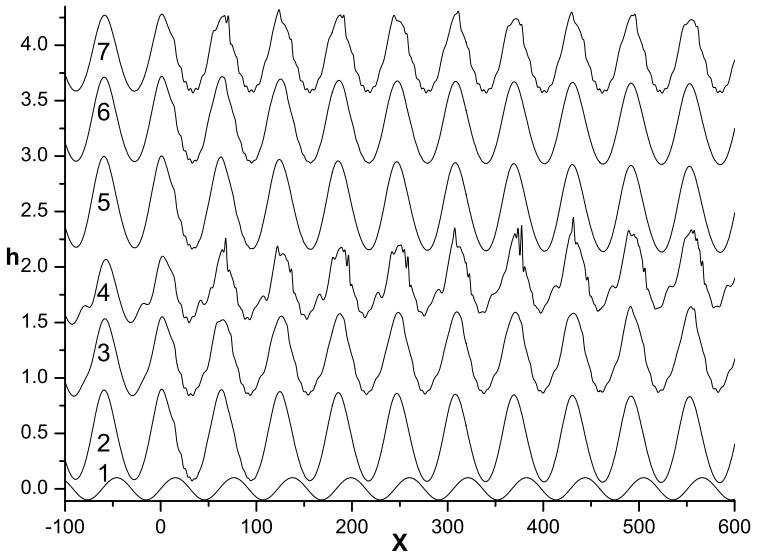

FIG. 8: The same as Fig. 7, but $L = 7$. The free surface response decreases with Ma. Resonance. Notice pure responses from $x =$ –100 to 0.

3.2 Results of Bi $= 1$

In the case of Bi $= 1$, the bumps in the free surface response are larger. Two examples of numerical calculations are presented to observe this phenomenon and its consequences. They correspond to a perturbation frequency $\omega = 0.5$ and $\omega = 2$.

3.2.1 Case for $\omega = 0.5$ and Re $= 1.391$

Here, despite the Biot number increase to Bi $= 1$, the wavenumbers remain above subcriticality. Then, for the frequency $\omega = 0.5$ and Re $= 1.391$, it is shown in Fig. 9 that the larger bump has an important influence on the free surface perturbations even when $L = 8$. For example, for $Q_C = 0.01$, the free surface perturbations almost have the same amplitude in the range of Ma. This is not only due to the bad conducting properties of the wall, it is also a consequence of the important change of the free surface response, which presents two notorious depressions which increase with Ma. Observe the contrast with the immediate increase in height of the other curves 5, 6, and 7 for $Q_C = 0.05$. This is a stabilizing effect of the surface response. When spatial resonance occurs at $L = 5$, Fig. 10 shows that it is easier to stabilize the free surface perturbations than in Fig. 4. It is important to note that also for Bi $= 1$, the increase of Ma decreases the amplitude of the free surface response. Again, this is a result of the sudden increase of the effective thermal conductivity of the wall around its thinnest part.

3.2.2 Case for $\omega = 2$ and Re $= 2.783$

Another example is give for $\omega = 2$ and Re $= 2.783$. The results are presented in Figs. 11 and 12. In Fig. 11 it is clear that the time-dependent perturbations have difficulty in saturating when $Q_C = 0.05$ and Ma $= 100$ (curve 7). This occurs despite that the wavenumbers are above the curve of subcriticality. Again, this is reflected in Fig. 12, where curve 7 is shown to be the exception when the other curves present spatial resonance (with $L = 8$) and therefore have effective stability. It is evident again that the relative height of the bump decreases with the increase of ω and Re, and that the stabilizing effect of the widening of the valley is not possible.

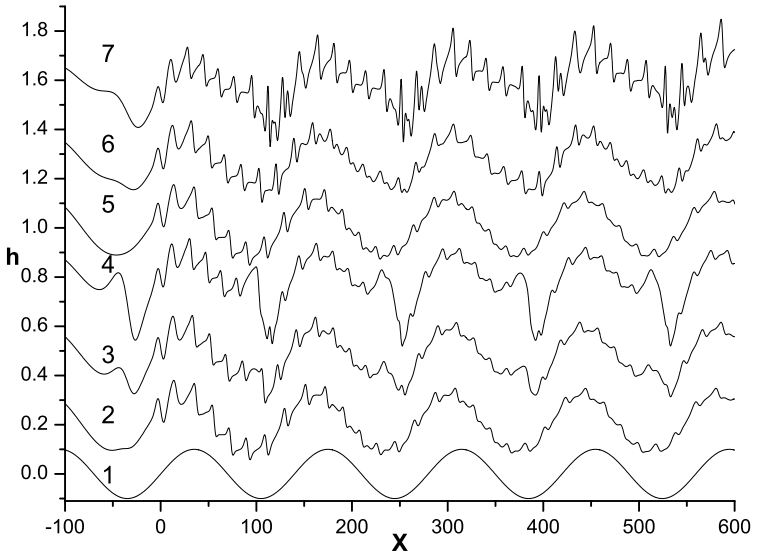

FIG. 9: Pr $= 7$, S $= 1$, Bi $= 1$, $d = 0.11$. $\omega = 0.5$, Re $= 1.391$, $L = 8$. (1) Wall. $Q_C = 0.01$: (2) Ma $= 10$, (3) Ma $= 50$, (4) Ma $= 100$. $Q_C = 0.05$: (5) Ma $= 10$, (6) Ma $= 50$, (7) Ma $= 100$. Notice pure responses from $x =$ –100 to 0.

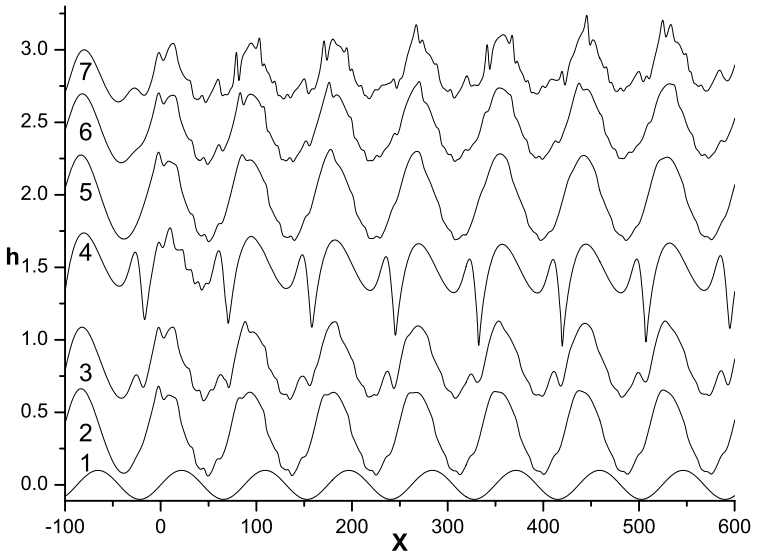

FIG. 10: The same as Fig. 9, but $L = 5$. The free surface response decreases with Ma. Resonance. Notice pure responses from $x =$ –100 to 0.

4. DISCUSSION

For all the numerical calculations, certain magnitudes of the parameters d and Q_C were selected. The thickness ratio d was selected small to avoid the stabilizing effects of large values of the ratio d/Q_C found in Dávalos-Orozco (2012). At the same time, the conductivity ratio was assumed small. This, of course, makes d/Q_C large but not very large.

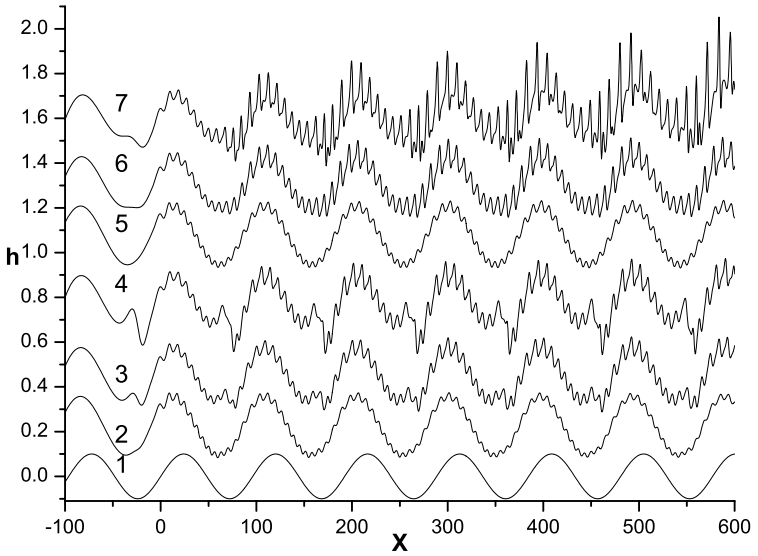

FIG. 11: Pr = 7, S = 1, Bi = 1, $d = 0.11$. $\omega = 2$, Re = 2.783, $L = 11$. (1) Wall. $Q_C = 0.01$: (2) Ma = 10, (3) Ma = 50, (4) Ma = 100. $Q_C = 0.05$: (5) Ma = 10, (6) Ma = 50, (7) Ma = 100. Notice pure responses from $x =$ –100 to 0.

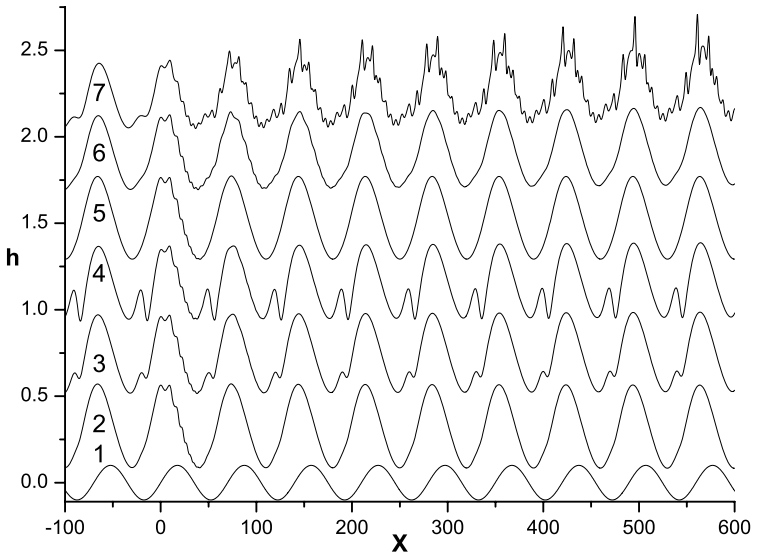

FIG. 12: The same as Fig. 11, but $L = 8$. The free surface response decreases with Ma. Resonance. Notice pure responses from $x =$ –100 to 0.

Fixing $d = 0.11$ and $Q_C = 0.01$ and 0.05 results in $d/Q_C = 11$ and 2.2, respectively. However, due to the wall waviness with amplitude $B = 0.1$, the parameter which appears in the denominator of the thermocapillary term of Eq. (19), $[\zeta(x) + d]/Q_C$ fluctuates, in one wavelength of the wall, between 1 and 21 for $Q_C = 0.01$ and between 0.2 and 4.2 for $Q_C = 0.05$. Thus the effectiveness of heat conduction changes from small to large in the span of a wall wavelength. When taking the spatial derivative of the thermocapillary term in Eq. (19), the terms with the derivatives

of $\zeta(x)$ will appear in the numerators. These terms are relevant when the ratio of the wavenumber of the wall over Q_C becomes important. These features of the problem are influential in the results presented in this paper.

It is found that when increasing Ma a bump appears in one or the other side of the valley of the free surface response. When L is large and far from spatial resonance, the bump appears to the left of the valley. When L decreases near to or into the spatial resonance, the bump appears to the right of the valley.

The reason for the appearance of the bump can be understood by looking carefully, for example, to the curves for Ma $= 100$ in Figs. 3 and 4. These curves show that near the thinner part of the wall a bump appears at the free surface response. Clearly, it is caused by the local increase of the thermocapillary terms when $[\zeta(x) + d]/Q_C$ decreases. In other words, it appears near to the place (the thinnest section) where the wall presents its largest effective heat conductivity. This bump seems to disappear when Q_C increases from 0.01 to 0.05. However, this is not the case. In fact, it is evident in curves 5, 6, and 7 of all the figures that the valley of the response is higher near the thinner part of the wall. This explains the amplitude decrease of the free surface response when Ma increases, in contrast with the numerical results of the Benney-type equation when $Q_C \to \infty$ (very good conducting wall) and calculated by Dávalos-Orozco (2013a). There, the amplitude of the free surface response increases with Ma. Thus the finite thickness and low conductivity of the wall are responsible for these phenomena.

The appearance of the bump to the left of the valley may be related to the bump found in experiments at the beginning of a heated plate (see, for example, Frank and Kabov, 2006; Kabova et al., 2014; and a review in Dávalos-Orozco, 2013a). However, it is unclear why the bump appears to the right of the valley when L is decreased until resonance is achieved.

Even though the amplitude of the response decreases with Ma, it is still possible to stabilized the time-dependent perturbations by means of spatial resonance, as observed in the figures for the smallest L used (with few exceptions in the range of parameters investigated). Naturally, the relatively bad conductivity of the wall helps to attain this goal.

An interesting phenomenon is found in Fig. 7 when $Q_C = 0.01$ and the magnitude of L is far from spatial resonance. That is, the amplitude of the time-dependent perturbations decreases when Ma increases from curve 2 to 4. This can be understood by observing the widening of valley when the response approaches the thinnest part of the wall. The width of the valley is so large due to the bump that the time-dependent perturbations remain for a long time and for a large space interval in a lower height region (locally thinner film). The consequence is that the local Reynolds number is reduced and the time-dependent perturbations decrease their amplitude even for large Ma (which at the same time produces a larger bump). It is important to point out, that this far from a resonance stabilizing effect of the widening of the valley, this is also a consequence of the increase of both the frequency of oscillation and the Reynolds number.

When Bi $= 1$, Fig. 9 shows that the influence of the bump on the stability of the time-dependent perturbations is important even for $L = 8$, far from resonance. Clearly, for $Q_C = 0.01$, the free surface perturbations nearly have the same amplitude in the range of Ma investigated (curves 2, 3, and 5). Here, the bad thermal conductivity of the wall is in part responsible. Another source of this interesting result is the large change which the free surface response suffers with the appearance of two valleys with depths increasing as Ma does. This also has a stabilizing effect, as is done by the widening of the valley of the free surface response. The results are in contrast with those of curves 5, 6, and 7 for $Q_C = 0.05$, where there is only one valley.

It is important to point out that numerical calculations have also been done for magnitudes of $Q_C > 0.05$. It is found that the amplitude of the free surface response is very similar but a little small in comparison to the results of the very good conducting wall of Dávalos-Orozco (2013a). The time-dependent perturbations, except for a slight change of phase, propagate in almost the same form. In this way, the decrease of d/Q_C leads to the results of the very good conducting wall.

The isothermal problem of Dávalos-Orozco (2007) deserves some discussion too. It is found that the free surface response for Ma $= 10$ and $Q_C = 0.01$ has almost the same amplitude as that of the isothermal problem. However, the time dependent perturbations have notable differences. The curves of the free surface response for Ma $= 50$ and 100 both have smaller amplitude than those of the isothermal case. If the conductivity ratio is increased to $Q_C = 0.05$, the amplitude of the response when Ma $= 10$ is larger than that in the isothermal problem (as expected). However, when Ma $= 50$ and 100 the response is smaller than when Ma $= 0$. In all cases the time-dependent perturbations differ from those of the isothermal problem.

Notice that the thermocapillary term of Eq. (19) does not depend on the angle of inclination. Therefore this has no influence on the Marangoni effect found when the thickness of the wall is very thin. A bump should appear for any angle of inclination.

An experiment is proposed using a mixture of 60% glycerol and 40% water. At 20°C its properties are $\rho = 1153.8$ kg/m^3, $\nu = 9.36 \times 10^{-3}$ m^2/s, $\sigma = 0.06764$ N/m, $-d\sigma/dT = 0.000096$ N/m°C, $k_f = 0.3805$ W/m°C, $H_h = 152$ W/m^2°C, and specific heat $c_p = 3096$ J/kg°C. The wall can be made with silica aerogel, a very bad conductor with $k_{\text{wall}} = 0.0145$ W/m°C and which can be made with thicknesses as small as 0.1 mm. Assuming $h_0 = 1.73 \times 10^{-3}$ m and $\varepsilon = 0.1$, then S = 3.858 and Re = 0.502, Pr = 87.8, Bi = 0.691, and $Q_C = 0.0381$ (between the 0.01 and 0.05 used here). The Ma value of the ratio Ma/Pr has to be adapted to the ratios Ma/7 used in the paper. Two magnitudes of $d/Q_c = 11$ and 2.2 were used with $d = 11$ $Q_C = 0.4191$ and $d = 2.2$ $Q_C = 0.0838$. Therefore, The ratio $d_{\text{wall}} = 0.4191$ $h_0 = 0.7250 \times 10^{-3}$ m and $d_{\text{wall}} = 0.0838$ $h_0 = 0.1449 \times 10^{-3}$ m.

5. CONCLUSIONS

An evolution equation in three dimensions was obtained to describe the time-dependent perturbations propagating on the free surface of a thin film flowing down a thick, badly conducting wavy wall subjected to a temperature gradient perpendicular to the film. It is shown that it is still possible to stabilize the perturbations by means of spatial resonance in the presence of thermocapillary effects. Surprising results were obtained in the free surface response to the wall deformations which are a consequence of the very thin section of the wall. An important result is found that the response amplitude decreases with the increase of the Marangoni number. In some cases the valley of the response widens in such a way that the time-dependent perturbations show some stabilization for certain frequencies and Reynolds numbers, even far away from L for resonance. Notice that due to the magnitude of the ratio d/Q_C, all the film instabilities investigated stay above the curve of subcriticality k_S, even though the Marangoni number is increased up to Ma = 100.

It is found that the film response is very similar to that of the isothermal flow for Ma = 10 because the wall is a bad conductor. But when Q_C is increased above the magnitudes used here, the film response becomes very similar to that of the very good conducting wall. Notice that the time-dependent perturbations differ in both cases.

It is shown again, under nonisothermal conditions, the importance that the wall topography has on the stability of thin films. Here it is demonstrated that the thickness of the wall also plays a significant roll, not only on the stability, but also on the free surface response which here presents extra deformations. Further research on this problem will be done, testing the thin film under different conditions.

ACKNOWLEDGMENTS

The authors would like to thank Joaquín Morales, Cain González, Alberto López, Raúl Reyes, Ma. Teresa Vázquez, and Oralia Jiménez for technical support.

REFERENCES

Ajaev, V. S., Instability and rupture of thin liquid films on solid substrates, *Interfacial Phenom. Heat Transfer*, vol. **1**, no. 1, pp. 81–92, 2013.

Alexeev, A., Gambaryan-Roisman, T., and Stephan, P., Marangoni convection and heat transfer in thin liquid films on heated walls with topography: Experiments and numerical study, *Phys. Fluids*, vol. **17**, no. 6, p. 062106, 2005.

Alleborn, N. and Raszillier, H., Local perturbation of thin film flow, *Arch. App. Mech.*, vol. **73**, no. 9, pp. 734–751, 2004.

Benney, D. J., Long waves on liquid films, *J. Math. Phys.*, vol. **45**, no. 2, pp. 150–155, 1966.

Bielarz, C. and Kalliadasis, S., Time-dependent free-surface thin film flows over topography, *Phys. Fluids*, vol. **15**, no. 9, pp. 2512–2524, 2003.

Bontozoglou, V. and Papapolymerou, G., Laminar film flow down a wavy incline, *Int. J. Multiphase Flow*, vol. **23**, no. 1, pp. 69–79, 1997.

Cao, Z., Vlachogiannis, M., and Bontozoglou, V., Experimental evidence for a short-wave global mode in film flow along periodic corrugations, *J. Fluid Mech.*, vol. **718**, pp. 304–320, 2013.

D'Alessio, S. J. D. Pascal, J. P., and Jasmine, H. A., Instability in gravity-driven flow over uneven surfaces, *Phys. Fluids*, vol. **21**, no. 6, p. 062105, 2009.

D'Alessio, S. J. D., Pascal, J. P., Jasmine, H. A., and Ogden, K. A., Film flow over heated wavy inclined surfaces, *J. Fluid Mech.*, vol. **665**, pp. 418–456, 2010.

Dávalos-Orozco, L. A., Davis, S. H., and Bankoff, S. G., Nonlinear instability of a fluid layer flowing down a vertical wall under imposed time-periodic perturbations, *Phys. Rev. E*, vol. **55**, no. 1, pp. 374–380, 1997.

Dávalos-Orozco, L. A. and Busse, F. H., Instability of a thin film flowing on a rotating horizontal or inclined plane, *Phys. Rev. E*, vol. **65**, no. 2, p. 026312, 2002.

Dávalos-Orozco, L. A., Nonlinear instability of a thin film flowing down a smoothly deformed surface, *Phys. Fluids*, vol. **19**, no. 7, p. 074103, 2007.

Dávalos-Orozco, L. A., Instabilities of thin films flowing down flat and smoothly deformed walls, *Microgravity Sci. Technol.*, vol. **20**, nos. 3-4, pp. 225–229, 2008.

Dávalos-Orozco, L. A., The effect of the thermal conductivity and thickness of the wall on the nonlinear instability of a thin film flowing down an incline, *Int. J. Non-Linear Mech.*, vol. **47**, no. 4, pp. 1–7, 2012.

Dávalos-Orozco, L. A., Stability of thin liquid films falling down isothermal and nonisothermal walls, *Interfacial Phenom. Heat Transfer*, vol. **1**, no. 2, pp. 93–138, 2013a.

Dávalos-Orozco, L. A., Stability of thin viscoelastic films falling down wavy walls, *Interfacial Phenom. Heat Transfer*, vol. **1**, no. 4, pp. 301–315, 2013b.

Deng, Q., Braun, R. J., Driscoll, T. A., and King-Smith, P. E., A model for the tear film and ocular surface temperature for partial blinks, *Interfacial Phenom. Heat Transfer*, vol. **1**, no. 4, pp. 357–381, 2013.

Frank, A. M. and Kabov, O. A., Thermocapillary structure formation in a falling film: Experiment and calculations, *Phys. Fluids*, vol. **18**, no. 3, p. 032107, 2006.

Gambaryan-Roisman, T. and Stephan, P., Flow and stability of rivulets on heated surfaces with topography, *J. Heat Transfer*, vol. **131**, no. 3, p. 033101, 2009.

Gambaryan-Roisman, T., Marangoni convection, evaporation and interface deformation in liquid films on heated substrates with non-uniform thermal conductivity, *Int. J. Heat Mass Transfer*, vol. **53**, nos. 1-3, pp. 390–402, 2010.

Gambaryan-Roisman, T., Yu, H. Y., Löffler, and Stephan, P., Long-wave and integral boundary layer analysis of falling film flow on walls with three-dimensional periodic structures, *Heat Transfer Eng.*, vol. **32**, nos. 7-8, pp. 705–713, 2011.

Gjevik, B., Ocurrence of finite-amplitude surface waves on falling liquid films, *Phys. Fluids*, vol. **13**, no. 8, pp. 1918–1925, 1970.

Hacker, T. and Uecker, H., An integral boundary layer equation for film flow over inclined wavy bottoms, *Phys. Fluids*, vol. **21**, no. 9, p. 092105, 2009.

Heining, C., Bontozoglou, V., Aksel, N., and Wierschem, A., Nonlinear resonance in viscous films on inclined wavy planes, *Int. J. Multiphase Flow*, vol. **35**, no. 1, pp. 78–90, 2009a.

Heining, C. and Aksel, N., Bottom reconstruction of thin film flow over topography: Steady solution and linear stability, *Phys. Fluids*, vol. **21**, no. 8, p. 083605, 2009b.

Heining, C. and Aksel, N., Effects of inertia and surface tension on a power-law fluid flowing down a wavy incline, *Int. J. Multiphase Flow*, vol. **36**, no. 11, pp. 847–857, 2010.

Heining C., Pollak T., and Aksel N., Pattern formation and mixing in three-dimensional film flow, *Phys. Fluids*, vol. **24**, no. 4, p. 042102, 2012.

Heining, C., Pollak, T., and Sellier, M., Flow domain identification from free surface velocity in thin inertial films *J. Fluid Mech.*, vol. **720**, pp. 338–356, 2013.

Joo, S. W., Davis, S. H., and Bankoff, S. G., Long-wave instabilities of heated falling films: Two-dimensional theory of uniform layers, *J. Fluid Mech.*, vol. **230**, pp. 117–146, 1991a.

Joo, S. W., Davis, S. H., and Bankoff, S. G., On falling-film instabilities and wave breaking, *Phys. Fluids*, vol. **3**, no. 1, pp. 231–232, 1991b.

Joo, S. W. and Davis, S. H., Instabilities of three-dimensional viscous falling films, *J. Fluid Mech.*, vol. **242**, pp. 529–547, 1992.

Kabova, Yu. O., Alexeev, A., Gambaryan-Roisman, T., and Stephan, P., Marangoni-induced deformation and rupture of a liquid film on a heated microstructured wall, *Phys. Fluids*, vol. **18**, no. 1, p. 012104, 2006.

Kabova, Yu., Kuznetsov,V. V., Kabov, O., Gambaryan-Roisman, T., and Stephan, P., Evaporation of a thin viscous liquid film sheared by gas in a microchannel, *Int. J. Heat Mass Transfer*, vol. **68**, pp. 527–541, 2014.

Kalliadasis, S., Bielarz, C., and Homsy, G. M., Steady free-surface thin film flows over topography, *Phys. Fluids*, vol. **12**, no. 8, pp. 1889–1898, 2000.

Lacanette, D, Gosset, A., Vincent, S. Buchlin, J. M., and Arquis, E., Macroscopic analysis of gas-jet wiping: Numerical simulation and experimental approach, *Phys. Fluids*, vol. **18**, no. 4, p. 042103, 2006.

Malamataris, N. A. and Bontozoglou, V., Computer aided analysis of viscous film flow along an inclined wavy wall, *J. Comp. Phys.*, vol. **154**, no. 2, pp. 372–392, 1999.

Negny, S., Meyer, M., and Prevost, M., Study of a laminar falling film flowing over a wavy wall column: Part I. NUmerical investigation of the flow pattern and coupled heat and mass transfer, *Int. J. Heat Mass Transfer*, vol. **44**, no. 9, pp. 2137–2146, 2001a.

Negny, S., Meyer, M., and Prevost, M., Study of a laminar falling film flowing over a wavy wall column: Part II. Experimental validation of hydrodynamic model, *Int. J. Heat Mass Transfer*, vol. **44**, no. 9, pp. 2147–2154, 2001b.

Ogden, K. A., D'Alessio, S. J. D., and Pascal, J. P., Gravity-driven flow over heated, porous, wavy surfaces, *Phys. Fluids*, vol. **23**, no. 12, p. 122102, 2011.

Oron, A., Bankoff, S. G. and Davis, S. H., Thermal singularities in film rupture, *Phys. Fluids*, vol. **8**, no. 12, pp. 3433–3435, 1996.

Oron, A. and Heining, C., Weighted-residual integral boundary-layer model for the nonlinear dynamics of thin films falling on an undulating vertical wall, *Phys. Fluids*, vol. **20**, no. 8, p. 082102, 2008.

Pascal, J. P. and D'Alessio, S. J. D., Instability in a gravity-driven flow over uneven permeable surfaces, *Int. J. Multiphase Flow*, vol. **36**, no. 6, pp. 449–459, 2010.

Pollak, T. and Aksel, N., Crucial flow stabilization and multiple instability branches of gravity-driven films over topography, *Phys. Fluids*, vol. **25**, no. 2, p. 024103, 2013.

Pozrikidis, C., The flow of a liquid film along a periodic wall, *J. Fluid Mech.*, vol. **188**, pp. 275–300, 1988.

Saprykin, S., Trevelyan, P. M. J., Koopmans, R. J., and Kalliadasis, S., Free-surface thin-film flows over uniformly heated topography, *Phys. Rev. E*, vol. **75**, no. 2, p. 026306, 2007.

Scheid B., Ruyer-Quil, C., Thiele, U., Kabov, O. A., Legros, J. C., and Colinet, P., Validity domain of the Benney equation including the Marangoni effect for closed and open flows, *J. Fluid Mech.*, vol. **527**, pp. 303–335, 2005.

Scholle, M., Wierschem, A., and Aksel, N., Creeping films with vortices over strongly undulated bottoms, *Acta Mech.*, vol. **168**, nos. 3-4, pp. 167–193, 2004.

Scholle, M., Haas, A., Aksel, N., Wilson, M. C. T., Thompson, H. M., and Gaskell, P. H., Competing geometry and inertial effects on local flow structure in thick gravity-driven fluid film, *Phys. Fluids*, vol. **20**, no. 12, p. 123101, 2008.

Shetty, S. and Cerro, R. L., Flow of a thin film over a periodic surface, *Int. J. Multiphase Flow*, vol. **19**, no. 6, pp. 1013–1027, 1993.

Trifonov, Y. Y., Viscous liquid film flows over a periodic surface, *Int. J. Multiphase Flow*, vol. **24**, no. 7, pp. 1139–1161, 1998.

Trifonov, Y. Y., Stability and nonlinear wavy regimes in downward film flows on a corrugated surface, *J. Appl. Mech. Tech. Phys.*, vol. **48**, no. 1, pp. 91–100, 2007a.

Trifonov, Y. Y., Stability of a viscous liquid film flowing down a periodic surface, *Int. J. Multiphase Flow*, vol. **33**, no. 11, pp. 1186–1204, 2007b.

Usha, R. and Uma, B., Long waves on a viscoelastic film flow down a wavy incline, *Int. J. Non-linear Mech.*, vol. **39**, no. 10, pp. 1589–1602, 2004.

Valluri, P., Matar, O. K., Hewitt, G. F., and Mendes, M. A., *Chem. Eng. Sci.*, vol. **60**, no. 7, pp. 1965–1975, 2005.

Veremieiev, S., Thompson, H. M., Scholle, M., Lee, Y. C., and Gaskell, P. H., Electrified thin film flow at finite Reynolds number on planar substrates featuring topography, *Int. J. Multiphase Flow*, vol. **44**, no. 1, pp. 48–69, 2012.

Wierschem, A., Scholle, M., and Aksel, N., Comparison of different theoretical approaches to experiments on film flow down an inclined wavy channel, *Exp. Fluids*, vol. **33**, no. 3, pp. 429–442, 2002.

Wierschem, A. and Aksel, N., Instability of a liquid film flowing down an inclined wavy plane, *Physica D*, vol. **186**, nos. 3-4, pp.

221–237, 2003.

Wierschem, A., Bontozoglou, V., Heining, C., Uecker, H., and Aksel, N., Linear resonance in viscous films on inclined wavy planes, *Int. J. Multiphase Flow*, vol. **34**, no. 6, pp. 580–589, 2008.

Wierschem, A., Pollak, C., Heining, C., and Aksel, N., Suppression of eddies in films over topography, *Phys. Fluids*, vol. **22** no. 11, p. 113603, 2010.

Zhao, L. and Cerro, R. L., Experimental characterization of viscous film flows over complex surfaces, *Int. J. Multiphase Flow*, vol. **18**, no. 4, pp. 495–516, 1992.